



Published in final edited form as:

*Neurosurgery*. 2011 August ; 69(2): 430–439. doi:10.1227/NEU.0b013e318212bcb4.

## Neuroendovascular Optical Coherence Tomography Imaging and Histological Analysis

Marlon S. Mathews, MD<sup>‡,§,\*</sup>, Jianping Su, PhD<sup>§,||,\*</sup>, Esmael Heidari, BS<sup>§,||</sup>, Elad I. Levy, MD<sup>†</sup>, Mark E. Linskey, MD<sup>‡</sup>, and Zhongping Chen, PhD<sup>§,||</sup>

<sup>‡</sup>Department of Neurological Surgery, University of California Irvine, Irvine, California

<sup>§</sup>Beckman Laser Institute and Medical Clinic, University of California Irvine, Irvine, California

<sup>||</sup>Department of Biomedical Engineering, University of California Irvine, Irvine, California

<sup>†</sup>Department of Neurosurgery, University at Buffalo, State University of New York, Buffalo, New York

### Abstract

**BACKGROUND**—Intravascular optical coherence tomography (OCT) is a recently developed optical imaging technique that provides high-resolution cross-sectional in situ images from intact tissue based on tissue reflectance of near-infrared or infrared light.

**OBJECTIVE**—To report on the feasibility of neuroendovascular OCT imaging and compare the neuroendovascular OCT findings with histology in nondiseased vessels in an animal, cadaveric, and clinical study.

**METHODS**—Catheter-based in vivo endovascular OCT imaging was performed in the common carotid arteries of 2 pigs and in the intracranial carotid arteries of 3 patients. The endovascular OCT device was delivered to the desired location via groin access and using standard endovascular procedures. Images were obtained via rotational and translational scanning using external motors. In vivo findings were reproduced using ex vivo OCT imaging in corresponding animal and human (cadaveric) harvested tissue segments. These segments underwent histological examination for comparison.

**RESULTS**—The structural compositions of the OCT-imaged segments of the common carotid arteries in pigs as well as the petrous and cavernous intracranial carotid arteries in patients were visualized at high resolution (8  $\mu$ m). The in vivo images were identical to those obtained ex vivo,

---

Copyright © 2011 by the Congress of Neurological Surgeons

Correspondence: Zhongping Chen, PhD, Beckman Laser Institute and Medical Clinic, 1002 Health Sciences Road, Irvine, CA 92612. z2chen@uci.edu.

\*These authors contributed equally to this article.

### Disclosure

This work was supported by research grants from the National Institutes of Health (EB-00293, CA-91717, EB-10090, and RR-01192), Air Force Office of Scientific Research (FA9550-04-1-01-01), and the Beckman Laser Institute Endowment. Dr Chen is a cofounder and director of OCT Medical Imaging and has ownership interests in and is a consultant to OCT Medical Imaging. Dr Mathews was supported by the UC Irvine Department of Neurological Surgery and UC Irvine Medical Center through a postgraduate research fellowship and has a significant ownership interest in Universal Coherence Imaging, LLC. Dr Levy receives research grant support (principal investigator: Stent-Assisted Re-canalization in acute Ischemic Stroke, SARIS), other research support (devices), and honoraria from Boston Scientific and research support from Codman & Shurtleff, Inc. and ev3/Covidien Vascular Therapies; has ownership interests in Intratech Medical Ltd. and Mynx/Access Closure; serves as a consultant on the board of Scientific Advisors of Codman & Shurtleff, Inc.; serves as a consultant per project and/or per hour for Codman & Shurtleff, Inc., ev3/Covidien Vascular Therapies, and TheraSyn Sensors, Inc.; and receives fees for carotid stent training from Abbott Vascular and ev3/Covidien Vascular Therapies. Dr Levy receives no consulting salary arrangements; all consulting is per project and/or per hour. The other authors have no personal financial or institutional interest in any of the drugs, materials, and devices described in this article.

demonstrating the imaging capabilities of the endovascular OCT device. The OCT images correlated well with the images obtained after histological sectioning and visualized in vivo the laminar vascular structure.

**CONCLUSION**—Neuroendovascular OCT imaging is feasible for clinical use and can detect with high resolution the structure of arterial segments. Understanding OCT imaging in nondiseased arteries is important in establishing baseline findings necessary for interpreting pathological processes. This allows neuroendovascular optical biopsies of vascular tissue to be obtained without the need for excision and processing.

### Keywords

Aneurysm; Brain; Neuroendovascular; Optical coherence tomography; Stroke

---

Intravascular optical coherence tomography (OCT) is a recently developed optical imaging technique that provides high-resolution cross-sectional in situ images from intact tissue based on tissue reflectance of near-infrared or infrared light.<sup>1,2</sup> The typical OCT image has an axial resolution of 8  $\mu\text{m}$  in tissue, which is at least 10 times higher than that of any clinically available diagnostic imaging modality.<sup>3</sup> Experiments correlating a limited number of excised coronary and aortic specimens with histology have demonstrated that OCT is capable of resolving microstructural features of atherosclerotic plaques (in human coronary vessels in situ and at autopsy).<sup>4-6</sup> Animal studies performed in vivo have demonstrated the use of an intravascular OCT catheter for directly imaging normal rabbit aortas and swine coronary arteries.<sup>7,8</sup> The unique capability of OCT to resolve micrometer-scale features of atherosclerosis makes this new imaging modality an attractive means for characterizing in vivo microstructural features of carotid plaques as well as those of intracranial vascular pathological processes such as aneurysms, dissections, stenosis, and fibromuscular dysplasia. The feasibility of intracoronary OCT imaging in patients has been previously described.<sup>6,9</sup> To date, however, this technology has never been investigated to assess feasibility for intracranial endovascular imaging in patients.

Before interpreting OCT images obtained from vascular pathology, it is important to accurately document in vivo and ex vivo OCT imaging findings in normal tissue. The purpose of this study was to establish baseline OCT findings in carotid and cerebrovascular arteries with respect to signal from various vessel wall components such as elastin, smooth muscle, and collagen as well as to assess the feasibility of in situ OCT imaging of the intracranial vasculature in patients, using standard angiographic techniques, and to study feasibility of intracranial delivery and imaging. The characterization of endovascular findings in this study was confirmed by correlating OCT images with histology images from animal tissue specimens and a human cadaveric tissue specimen. The first demonstration of intracranial endovascular OCT imaging in patients is reported.

## METHODS

### Study Overview

Our study began with the development of a device that could be attached to the OCT unit and could be used for access to and imaging of cerebral vessels. We tested the device first in vivo in the common carotid arteries (CCAs) of pigs, followed by ex vivo testing in pig carotid arteries and rabbit aortas where comparisons were made of OCT imaging findings with histological findings. Once imaging findings were found to satisfactorily correlate, the intracranial carotid arteries (ICAs) of human subjects were imaged in a clinical study. Finally, we obtained OCT and histological images from human cadaveric ICA segments to compare our in vivo clinical imaging findings with the ex vivo OCT imaging findings and

histological findings from human cadavers. This study was conducted with the approval of the institutional review board and the institutional animal care and use committee at the University of California Irvine.

### **OCT Equipment**

The OCT equipment used for the study consisted of a time-domain OCT system previously described by Zhao et al<sup>10</sup> and Ren et al<sup>11</sup> (the unit was built in our laboratory and was not a commercial unit). The time delay of light backscattered from the sample is measured by a fiber-based Michelson interferometer. A 1310-nm, partially coherent light source with a full-width-at-half-maximum bandwidth of 75 nm was used as the light source. The axial line scanning rate was 500 Hz. The axial resolution in tissue was 8  $\mu\text{m}$ .

### **Endovascular OCT Device**

The design and construct of the endovascular OCT device were previously described.<sup>12</sup> Briefly, the main structural components of the OCT device included U.S. Food and Drug Administration–approved endovascular devices, such as guidewires. The OCT device had an outer diameter of 0.036-inch proximally and 0.018-inch distally at the tip (Figure 1). The device was sterilized using high-temperature plasma sterilization (Sterrad Sterilization System, Advanced Sterilization Products, division of Ethicon, Inc, a Johnson & Johnson Company, New Brunswick, New Jersey).

### **Animal Study**

Endovascular OCT imaging was performed bilaterally in the CCAs of 2 anesthetized (isoflurane) adolescent farm pigs (weighing approximately 50 kg each). In vivo OCT images were obtained and analyzed via linear and rotational scanning using an external motor. Immediately after euthanasia (with isoflurane anesthesia); the same arterial regions were harvested and ex vivo OCT images were obtained from the same specimen. In addition, ex vivo samples of the abdominal aorta of adult rabbits obtained immediately after euthanasia (with isoflurane anesthesia) were imaged using linear and rotational scanning OCT.

### **In Vivo OCT Imaging Procedure**

The endovascular OCT device was delivered at the artery of interest using standard endovascular techniques under fluoroscopic guidance. Once the tip of the device was in a satisfactory position, as imaged with fluoroscopy, OCT images were acquired at a rate of 1 frame per second (512 angular pixels  $\times$  512 radial pixels), displayed with a gray-scale lookup table, and digitally archived. Linear and rotational transduction of the catheter was performed by using an external linear stage (Newport Inc, Irvine, California) and a rotational motor (Animatics Inc, Irvine, California).

Because blood interferes with OCT imaging quality, saline solution flushes were used during in vivo OCT imaging. Although proximal balloon occlusion during OCT imaging has been described as a technique to limit blood interference,<sup>13</sup> we elected not to use proximal balloon occlusion. The required volume and rate of flushing were adjusted according to the blood flow in the parent vessel at the site of OCT imaging. During the clinical study (described in the following), we used 5- to 10-mL bolus saline solution flushes through a 5-French sheath that was placed proximally in the ipsilateral ICA. During in vivo imaging of the CCAs in the pigs, we used 10- to 20-mL bolus flushes.

### **Elastase Protocol**

Segments approximately 0.5 inch in length of the pig CCAs that were excised surgically were incubated ex vivo in 0.4 U/mL porcine pancreatic elastase (Worthington Biochemical

Corporation, Lakewood, New Jersey) for 4 hours at room temperature. OCT imaging was then performed in these segments using linear and rotational scanning. After OCT imaging, the elastase-incubated CCA segments were fixed in formalin and underwent histological examination as described in the following.

In addition, approximately 0.5-inch-long adjacent segments of rabbit aorta that were excised surgically were incubated *ex vivo* in 2 petri dishes as follows. One petri dish (experimental sample) contained 0.4 U/mL porcine pancreatic elastase (Worthington Biochemical Corporation), whereas the other (control sample) contained normal saline solution. OCT imaging of both samples was obtained after 2- and 4-hour incubation periods at room temperature in each petri dish. After the 4-hour incubation period, both samples were fixed in formalin and underwent histological examination as described in the following sections.

### **Clinical OCT Imaging**

We examined the feasibility of intracranial OCT imaging in patients using femoral artery access to deliver the endovascular OCT device. Delivery of the device was performed using standard angiographic techniques and standard delivery sheaths and catheters. Endovascular OCT imaging of the intracranial ICA (petrous and cavernous segments) was performed in 3 patients undergoing diagnostic angiograms. OCT imaging was performed in nondiseased vessel segments (Figure 2, A and B). All patients were adults with previously coiled cerebral aneurysms and had returned for routine postprocedure angiograms at 6 months, at which time the OCT imaging procedure was performed.

### **Human Cadaveric Study**

Adjacent 1-cm long segments of the petrous and cavernous ICA were harvested from a formalin-fixed human cadaver head. *Ex vivo* OCT imaging was performed in the human cadaveric specimen using OCT. Explanted cadaveric arterial segments corresponding to the locations imaged in the patients were imaged intraluminally with an OCT catheter. Subsequently, the imaged cadaveric segments were carefully marked and fixed in formalin and underwent sectioning and staining for histological examination, as described in the following.

### **Histological Examination**

After OCT imaging, the image segments of animal and cadaveric tissue were processed using routine histological techniques. Briefly, arterial segments were fixed in 10% formalin and processed in standard paraffin embedding. Sections (5- $\mu$ m thick) of the embedded segments were then cut at the marked imaging sites and stained with trichrome stain for elastin, collagen, and smooth muscle (Sigma-Aldrich Manufacturing LLC, St. Louis, Missouri).

### **Correlation Between OCT Images And Histology**

Because a goal of the study was to describe baseline OCT imaging findings in normal vasculature rather than imaging-specific pathology, nondiseased segments of blood vessels were scanned using OCT and compared with normal histological findings in the same arteries. Similarly, OCT imaging findings after elastase incubation were correlated with histological findings in the same arteries. Thus, OCT imaging and histology were compared for structural morphology. No pathological regions were studied or identified.

## RESULTS

### Baseline Animal Findings

In vivo OCT imaging of the pig CCAs showed all vascular structural components including the intima and internal elastic lamina (IEL), media, external elastic lamina (EEL), and adventitia (Figure 3, A–D). The same findings were reproduced with ex vivo OCT imaging of both CCAs (Figure 3E). Histological examination of the pig CCAs showed the OCT findings to correlate well with histological findings, with good resolution (Figure 3F). Rabbit aorta imaging at baseline (Figure 4, A and B) showed an area of high signal similar to what was seen intracranially in patients. Histological examination of the rabbit aorta showed this area of high signal to correspond to the thick layer of medial elastin fibers, the aorta being an elastic artery (Figure 4C).

### Animal Imaging Findings After Elastase Incubation

The OCT imaging of the pig CCA segments revealed a loss of high signal from the IEL and EEL (Figure 5A). This was clearly seen on the histology (Figure 5B). Incubation of the vascular segments in elastase for 4 hours effectively destroyed all the elastin in the arterial walls.

OCT images obtained after incubation of the rabbit aorta specimen in porcine pancreatic elastase for 2 hours showed a thin, bandlike clear lucency near the luminal surface of the vessel; this lucency was not detected on the control specimen incubated during the same period in normal saline solution (Figure 5, C and D). Incubation of the rabbit aorta specimen in elastase for 4 hours was associated with a complete breakdown of vascular tissue structure with loss of elastin on histological images (Figure 6, A and B). This was detected with OCT imaging (Figure 6C).

### Clinical Findings

The endovascular OCT device was successfully delivered intracranially in all 3 patients using standard endovascular techniques after arterial access was obtained via a femoral approach. OCT images of the cavernous ICA in vivo showed a thick band of high signal near the luminal surface of the artery, followed by a discrete reduction in signal intensity on the adventitial side (Figure 7, A and B); the vessel scanned is shown in the angiogram in Figure 7C. The same findings were found in the petrous carotid artery. All patients remained neurologically intact after the OCT imaging procedure. Magnetic resonance (MR) imaging, including diffusion-weighted images and apparent diffusion coefficient maps were obtained in the first patient post-procedure (who reported headache during the procedure) and showed no evidence of ischemia (images not shown). No procedural complications occurred.

### Human Cadaveric OCT Findings

Ex vivo OCT imaging of the human cadaveric cavernous and petrous ICA (Figure 8, A–D) showed a thick band of high signal in the luminal side of the vessel wall, similar to what was observed in the clinical OCT imaging study. Histological examination showed this area of high signal to correspond to the elastin and smooth muscle layers of the media (Figure 8, E and F).

## DISCUSSION

Cerebrovascular disease and strokes are among the leading causes of death and disability in our population. A significant proportion of strokes arise from a proximal or local arterial source with preexisting arterial pathology. Imaging of intra-arterial vascular pathology should provide information of both diagnostic and therapeutic value. Conventional

diagnostic imaging modalities such as catheter angiography, ultrasonography, computed tomography angiography, MR imaging, and MR angiography provide luminal macrostructural and flow-related information with typical imaging resolutions in the millimeter range. These modalities provide limited information on vessel wall structural pathology outside of luminal alterations. Recently, high-frequency intravascular ultrasound devices have become available that provide better resolution imaging on the order of 100 to 150  $\mu\text{m}$ . Studies have shown intravascular ultrasound to be superior to angiography with respect to plaque characterization, stent deployment,<sup>14,15</sup> and correlation between plaque features and acute coronary syndrome.<sup>16</sup>

More recently, intravascular OCT has been shown to provide high-resolution cross-sectional images of tissue *in situ*.<sup>3</sup> OCT measures the amplitude of backscattered light (optical echoes or reflectance) returning from a near-infrared or infrared light source directed at the arterial wall as a function of delay. *Ex vivo* studies have shown resolution capabilities of 2 to 10  $\mu\text{m}$  (near-histological resolutions), which provide the necessary definition to image areas of vascular wall pathology such as the thin fibrous caps, lipid-rich areas, and macrophage content in vulnerable atherosclerotic plaques.<sup>3,6,17,18</sup> Studies have shown OCT to be capable of detecting several different features of intravascular pathology, such as the disruption of the fibrous cap of lipid-rich plaques, the presence of intracoronary thrombus, the depth of dissections caused by balloon inflations, the cuts in atherosclerotic plaque made by the blades of a cutting balloon, tissue protruding through stent struts, and underdeployed struts otherwise missed by intravascular ultrasound.<sup>16</sup>

The goals of our study were to develop a method for intracranial delivery and imaging of an endovascular OCT device and to establish baseline OCT findings in nondiseased carotid and cerebral vasculature. For this, the endovascular OCT device had to be small (<1 mm in diameter) and have mechanical, biological, radiological, and optical properties necessary for safe and reproducible intracranial delivery. The device needed to have proximal control and maneuverability, with efficient optical and mechanical transduction. It needed to be radiopaque so that the operator could verify its position on fluoroscopy. We were able to incorporate an optical fiber into a hybrid device made up of endovascular guidewires (diameters of 0.46 mm and 0.91 mm) with a proximal steel wire core. With this arrangement, the endovascular OCT device was soft and flexible at the tip and firm and maneuverable from its proximal end. The proximal end was connected to an external motor for rotational or linear mechanical translation. With this arrangement, we were able to demonstrate the feasibility of intracranial imaging with no adverse events in 3 patients.

We were also interested in characterizing the OCT signals arising from elastin and the tunica media. Such characterization is of particular applicability in the imaging of intracranial aneurysms. Arteries at the base of the brain lack the structural protection of the EEL seen in the more proximal extracranial portions of these arteries. Intracranial saccular aneurysms arise as abnormal outpouchings of arterial walls seen most commonly at arterial branch points at the circle of Willis. Etiologically, they are thought to be related to congenital or acquired structural defects at these branch points. These defects commonly involve the absence of an IEL or media (medial cushion defect).<sup>19,20</sup> These aneurysms rupture in some patients, with the risk of rupture only roughly correlating with the aneurysm diameter (>1 cm).<sup>21</sup> Despite this correlation, the majority of ruptured aneurysms encountered in clinical practice are less than 1 cm in diameter. Clearly, an objective assessment of aneurysm wall structure could lead to more sensitive and useful modeling of aneurysm rupture risk. In this study, we demonstrate the capability of OCT to detect the IEL, EEL, and medial cushion *in vivo* (Figures 3 and 7). Thus, with further study, OCT may hold the promise of evaluating intracranial aneurysms structurally and assessing risk of rupture based on structural information, such as the presence or absence of IEL, density and orientation of elastin and



collagen fibers, the presence of medial cushion defects, and visualization of microscopic dissections and tears.

The OCT imaging findings in our study correlated well with structural information obtained in the same vessel segments through histological examination (Figures 3–6 and 8). This was confirmed in the intracranial, carotid, and aortic arterial segments, each with a different structural anatomy. Loss of elastin in both segments gave rise to parallel findings on OCT imaging (Figures 5 and 6). In vivo imaging findings were at least as good as the imaging information obtained ex vivo and were highly reproducible, demonstrating the effectiveness and efficiency of the endovascular OCT device construct. Although only 1 representative image from each imaging session is shown here, 5 to 20 images were obtained during each session. In vivo and ex vivo images obtained from arterial segments in patients and animals were identical, demonstrating the reproducibility of the imaging findings.

## CONCLUSION

Intracranial OCT imaging can be safely performed in patients with appropriately engineered endovascular OCT devices. The signal obtained from our device is of sufficient quality to resolve the circumferential cross-sectional structural composition of intracranial arteries from within the lumen. Imaging information gathered from the in vivo application of the device closely correlates with histological information in normal vasculature. Endovascular OCT may be particularly effective and attractive for detecting and analyzing special features of complex vascular pathology, such as arterial plaques and aneurysms. Structural changes, such as loss of elastic laminae and medial cushion defects seen in intracranial aneurysms and other intracranial pathological conditions, can now be assessed endovascularly in vivo in patients with minimally invasive OCT imaging using nonionizing radiation (light). Potentially more useful and relevant means for modeling aneurysm rupture risk based on lesion-specific cross-sectional structural information are on the horizon.

## Acknowledgments

We thank Paul H. Dressel, BFA, for preparation of the illustrations and Debra J. Zimmer, AAS, CMA-A, for editorial assistance. Presented in part at the following meetings: International Stroke Conference, San Francisco, California, February 7–9, 2007, and the American Society for Neuroradiology 45th Annual Meeting and Neuroradiology Education and Research Foundation Symposium, Chicago, Illinois, June 9–14, 2007.

## ABBREVIATIONS

<b>CCA</b>	common carotid artery
<b>EEL</b>	external elastic lamina
<b>ICA</b>	internal carotid artery
<b>IEL</b>	internal elastic lamina
<b>OCT</b>	optical coherence tomography

## References

1. Fujimoto JG, Brezinski ME, Tearney GJ, et al. Optical biopsy and imaging using optical coherence tomography. *Nat Med.* 1995; 1(9):970–972. [PubMed: 7585229]
2. Huang D, Swanson EA, Lin CP, et al. Optical coherence tomography. *Science.* 1991; 254(5035): 1178–1181. [PubMed: 1957169]
3. Yabushita H, Bouma BE, Houser SL, et al. Characterization of human atherosclerosis by optical coherence tomography. *Circulation.* 2002; 106(13):1640–1645. [PubMed: 12270856]

4. Brezinski ME, Tearney GJ, Bouma BE, et al. Imaging of coronary artery microstructure (in vitro) with optical coherence tomography. *Am J Cardiol.* 1996; 77(1):92–93. [PubMed: 8540467]
5. Brezinski ME, Tearney GJ, Bouma BE, et al. Optical coherence tomography for optical biopsy. Properties and demonstration of vascular pathology. *Circulation.* 1996; 93(6):1206–1213. [PubMed: 8653843]
6. Jang IK, Bouma BE, Kang DH, et al. Visualization of coronary atherosclerotic plaques in patients using optical coherence tomography: comparison with intravascular ultrasound. *J Am Coll Cardiol.* 2002; 39(4):604–609. [PubMed: 11849858]
7. Fujimoto JG, Boppart SA, Tearney GJ, Bouma BE, Pitris C, Brezinski ME. High resolution in vivo intra-arterial imaging with optical coherence tomography. *Heart.* 1999; 82(2):128–133. [PubMed: 10409522]
8. Tearney GJ, Jang IK, Kang DH, et al. Porcine coronary imaging in vivo by optical coherence tomography. *Acta Cardiol.* 2000; 55(4):233–237. [PubMed: 11041121]
9. Jang IK, Tearney G, Bouma B. Visualization of tissue prolapse between coronary stent struts by optical coherence tomography: comparison with intravascular ultrasound. *Circulation.* 2001; 104(22):2754. [PubMed: 11723031]
10. Zhao Y, Chen Z, Saxer C, Xiang S, de Boer JF, Nelson JS. Phase-resolved optical coherence tomography and optical Doppler tomography for imaging blood flow in human skin with fast scanning speed and high velocity sensitivity. *Opt Lett.* 2000; 25(2):114–116. [PubMed: 18059800]
11. Ren H, Ding Z, Zhao Y, Miao J, Nelson JS, Chen Z. Phase-resolved functional optical coherence tomography: simultaneous imaging of in situ tissue structure, blood flow velocity, standard deviation, birefringence, and Stokes vectors in human skin. *Opt Lett.* 2002; 27(19):1702–1704. [PubMed: 18033341]
12. Su JY, Mathews MS, Nwagwu CI, et al. Imaging treated brain aneurysms in vivo using optical coherence tomography. *Proc SPIE.* 2008; 6847:684732.
13. Kawase Y, Hoshino K, Yoneyama R, et al. In vivo volumetric analysis of coronary stent using optical coherence tomography with a novel balloon occlusion-flushing catheter: a comparison with intravascular ultrasound. *Ultrasound Med Biol.* 2005; 31(10):1343–1349. [PubMed: 16223637]
14. Fitzgerald PJ, Oshima A, Hayase M, et al. Final results of the Can Routine Ultrasound Influence Stent Expansion (CRUISE) study. *Circulation.* 2000; 102(5):523–530. [PubMed: 10920064]
15. Pasterkamp G, Schoneveld AH, van der Wal AC, et al. Relation of arterial geometry to luminal narrowing and histologic markers for plaque vulnerability: the remodeling paradox. *J Am Coll Cardiol.* 1998; 32(3):655–662. [PubMed: 9741507]
16. Yamagishi M, Terashima M, Awano K, et al. Morphology of vulnerable coronary plaque: insights from follow-up of patients examined by intravascular ultrasound before an acute coronary syndrome. *J Am Coll Cardiol.* 2000; 35(1):106–111. [PubMed: 10636267]
17. MacNeill BD, Lowe HC, Takano M, Fuster V, Jang IK. Intravascular modalities for detection of vulnerable plaque: current status. *Arterioscler Thromb Vasc Biol.* 2003; 23(8):1333–1342. [PubMed: 12805071]
18. Tearney GJ, Yabushita H, Houser SL, et al. Quantification of macrophage content in atherosclerotic plaques by optical coherence tomography. *Circulation.* 2003; 107(1):113–119. [PubMed: 12515752]
19. Forbus WD. On the origin of military aneurysms of the superficial cerebral arteries. *Bull Johns Hopkins Hosp.* 1930; 47:239–284.
20. Hassler O. Media defects in the cerebral arteries: differences in microscopical structure between neonates and adults. *Acta Neuropathol.* 1962; 1(5):514–518.
21. Wiebers DO, Whisnant JP, Huston J III, et al. Unruptured intracranial aneurysms: natural history, clinical outcome, and risks of surgical and endovascular treatment. *Lancet.* 2003; 362(9378):103–110. [PubMed: 12867109]



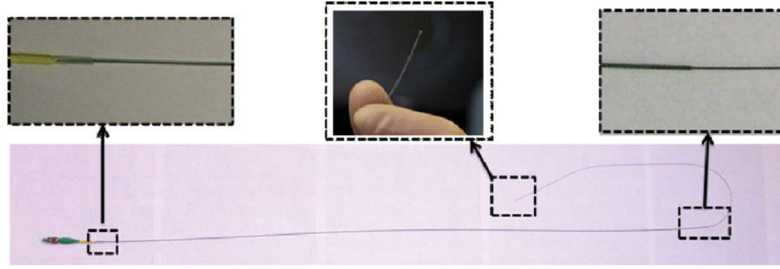


**FIGURE 1.**

Endovascular optical coherence tomography device showing its proximal end (left), distal tip (center), and junction of the coiled wires (right). Reproduced with permission from Su JY, Mathews MS, Nwagwu CI, et al. Imaging treated brain aneurysms in vivo using optical coherence tomography. *Proc SPIE*. 2008;6847:684–732.<sup>12</sup>

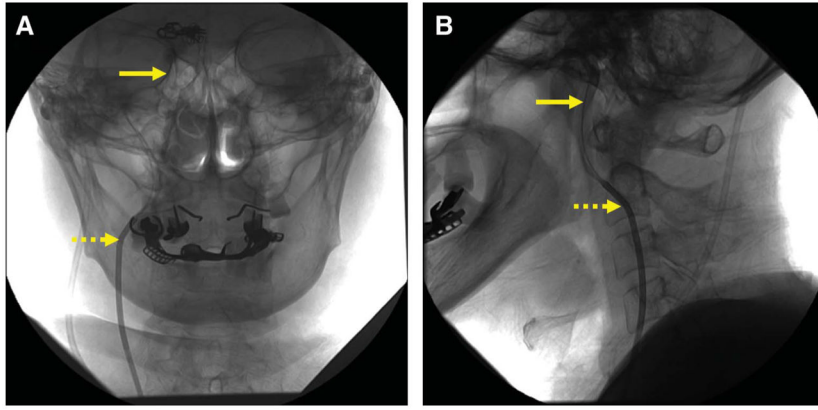


**FIGURE 2.**

Angiographic images, anteroposterior (**A**) and lateral (**B**) projections, in a patient with the optical coherence tomography (OCT) device in situ (solid arrows). Dashed arrows indicate the proximal sheath housing the OCT device. **A**, reproduced with permission from Su JY, Mathews MS, Nwagwu CI, et al. Imaging treated brain aneurysms in vivo using optical coherence tomography. *Proc SPIE*. 2008;6847:684732.<sup>12</sup>

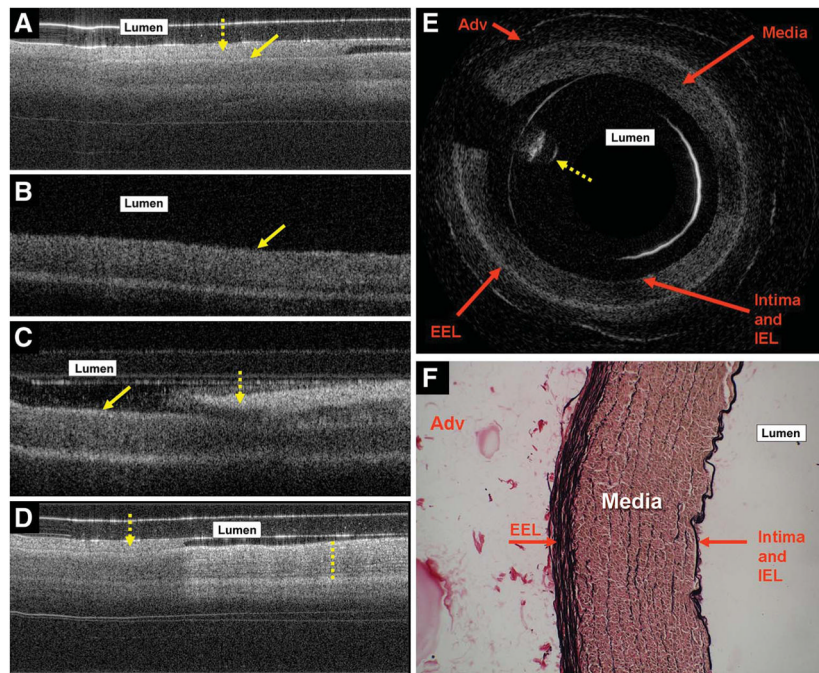


**FIGURE 3.**

**A**, endovascular optical coherence tomography (OCT) image obtained in vivo from the left common carotid artery (CCA) of a pig. Arrows indicate the endothelial surface (solid arrow) and luminal blood (dashed arrow). Blood, because of high absorption and scattering of near-infrared light, shows up as a high OCT signal in the lumen, obscuring the OCT signal from the vessel wall. **B**, endovascular OCT image of the same artery obtained immediately after saline solution flush shows dilation of the vascular lumen with the vessel wall being pushed outward. Blood is no longer visible in the vascular lumen. The thin, high-signal strip on the surface corresponds to the intima and internal elastic lamina (IEL) seen later in histological images. Moving outward in the vessel wall, the IEL is followed by a low-signal band corresponding to the media, a high-signal strip corresponding to the EEL, and a low-signal area corresponding to the adventitia (Adv) on histological images. Solid arrow indicates the endothelial surface. **C**, after the flush, blood (dashed arrow) re-enters the lumen. Solid arrow indicates the endothelial surface. **D**, in vivo endovascular OCT image captured during a saline solution flush (direction of flush is from right to left in the figure) in the right CCA of a pig showing good vascular structural detail on the right side of the image, which is filled with luminal saline solution, whereas the left side of the image has luminal blood. The dashed line (on the right side of this image) shows structural detail in the tunica media as stripes of high signal. These stripes correspond well to elastin fibers in the media, as seen on histology. Dashed arrow indicates luminal blood. **E**, ex vivo OCT image of the left CCA of a pig obtained using rotation scanning OCT showing vascular structural details that correspond well to the in vivo images and histology. The dashed arrow corresponds to guidewire artifact that is seen during rotational OCT scanning. **F**, histological images (magnification  $\times 200$ ) showing vascular structure stained with trichrome stain. The elastin is stained black; collagen, pink; and smooth muscle, brown. Because the endovascular OCT device contains glass components that cause light scattering and reflection, high-signal artifacts are seen as 1 or 2 lines in the vessel lumen.

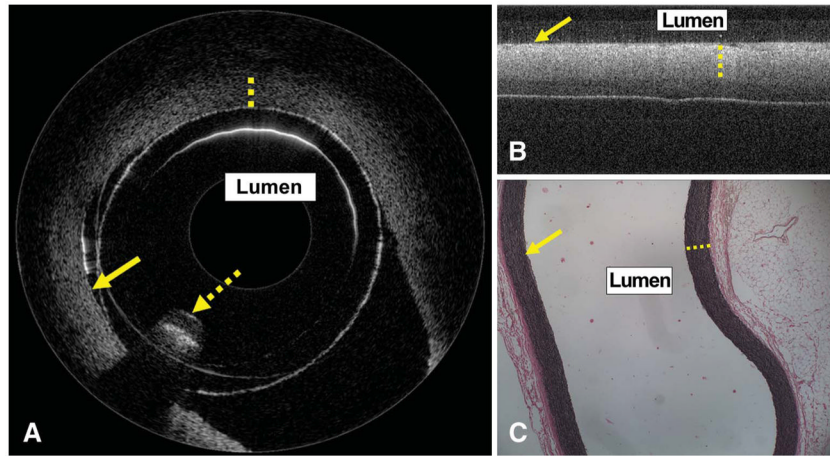


**FIGURE 4.**

Ex vivo images obtained from a rabbit aorta using rotational (A) and linear scanning (B). The dashed lines in A through C show high-signal bands that correspond to the elastic media seen on histology (C). Arrows in A through C indicate the endothelial surface of the aorta. The dashed arrow in A corresponds to guidewire artifact seen during rotational scanning.

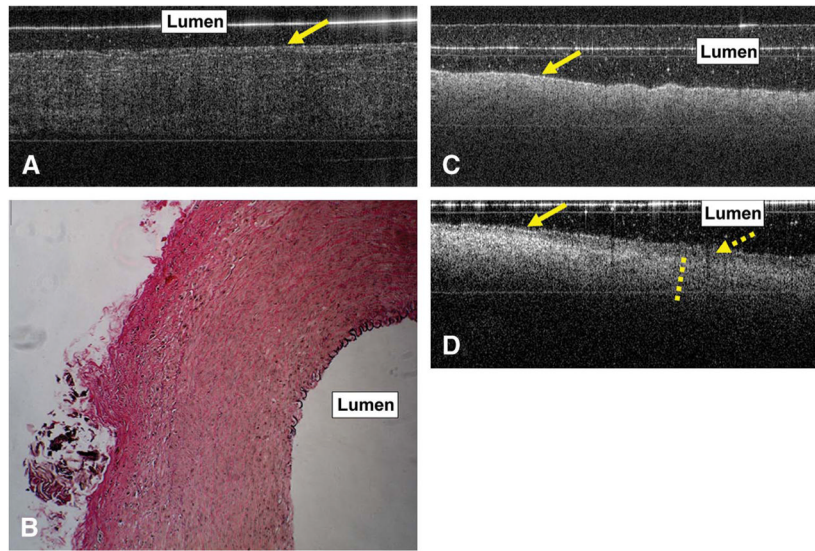


**FIGURE 5.**

Ex vivo optical coherence tomography (OCT) image of the pig left common carotid artery (CCA) obtained after 4-hour elastase incubation (**A**). The arrow indicates the luminal surface of the vessel. The OCT image shows loss of high signal that corresponds to the internal elastic lamina (IEL) and external elastic lamina (EEL). There is loss of the layered vessel wall structure. Histological images (magnification  $\times 200$ ) confirm these findings with loss of elastin from the IEL, media, and EEL (**B**). The OCT and histological findings were highly reproducible in multiple scanned sections of the left and right CCAs. Ex vivo OCT image obtained after 2-hour incubation of rabbit aorta segments in saline solution (**C**) and porcine pancreatic elastase (**D**). **C**, baseline OCT imaging findings with the band of high signal correspond to elastin, as shown in Figure 4A and B (**D**). An area of low signal (dashed arrow) is seen in the luminal side of the vessel, probably secondary to elastin breakdown. Outside the area of low signal is the thick band of high signal (dashed line). The solid arrows in **C** and **D** indicate the luminal surface of the aorta.



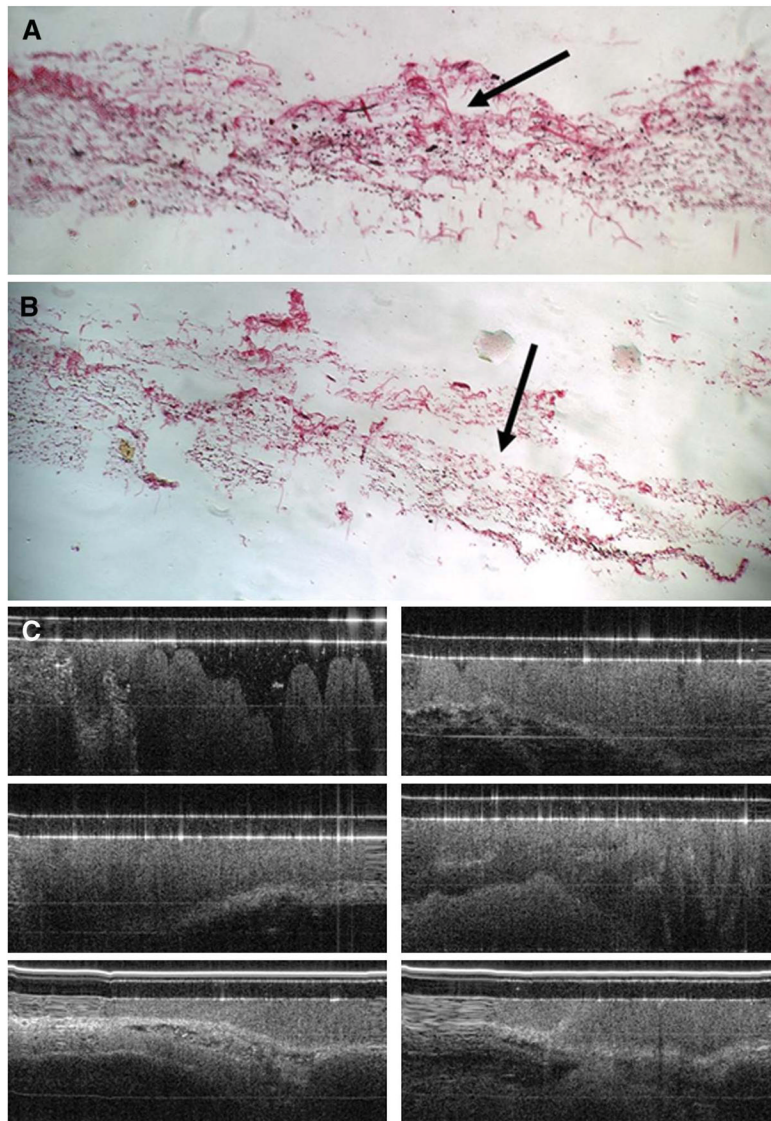


**FIGURE 6.** Histological images (magnification  $\times 200$ ) of the rabbit aorta obtained after 4-hour incubation with elastase enzyme (**A** and **B**). Images show loss of elastin and breakdown of the architecture of the aortic tissue (compare with Figure 4C). Arrows indicate the aortic lumen. **C**, 6 representative ex vivo optical coherence tomography images obtained from the rabbit aorta after incubation in elastase for 4 hours showing breakdown of tissue architecture with mixed low- and high-signal areas.



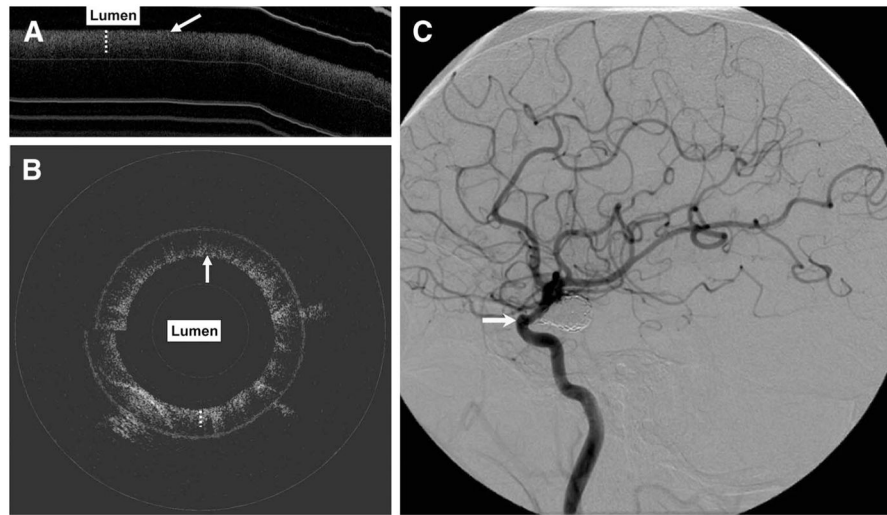


**FIGURE 7.** In vivo optical coherence tomography (OCT) images obtained from the cavernous internal carotid artery (ICA) using linear (**A**) and rotational (**B**) scanning in a patient. The endothelial surface begins at the tip of the arrows (in **A** and **B**). A thick band of high signal (dotted lines) is on the endothelial side of the vessel. **C**, lateral projection angiographic image with the arrows indicating the region of the cavernous ICA (solid arrow) scanned for OCT imaging. Note the coiled aneurysm immediately distal to the imaged section.

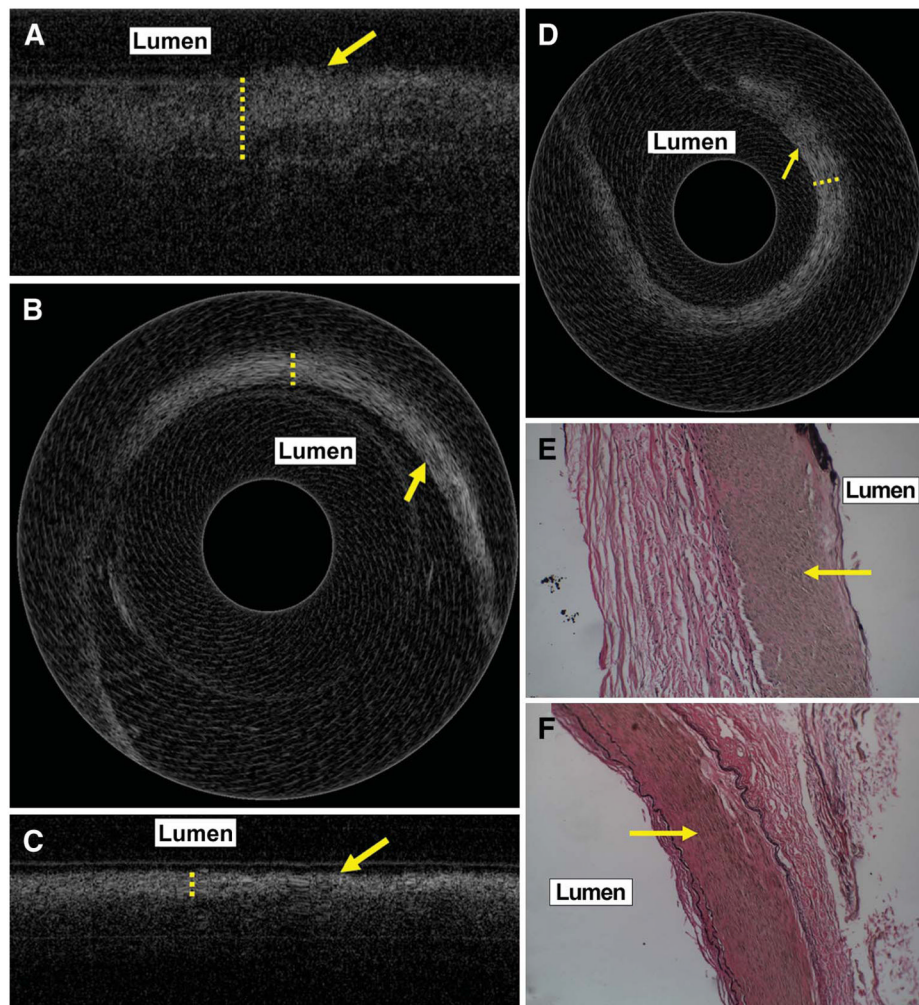


**FIGURE 8.**

Ex vivo linear and rotational scanning images obtained from cadaveric cavernous internal carotid artery (ICA) (**A** and **B**) and petrous ICA (**C** and **D**) showing a thick band of high signal (dotted lines) on the endothelial side, similar to the in vivo clinical findings in Figure 5. The arrows in **A** to **D** indicate the endothelial surface. Histological images (magnification  $\times 200$ ) stained with trichrome stain for elastin show this band of high signal to correspond to the media (arrow) of the corresponding regions of the cavernous (**E**) and petrous ICA (**F**).